

Threading Polystyrene Stars: Impact of Star to POM-POM and Barbwire Topology on Melt Rheological and Foaming Properties

Marie-Christin Röpert, Anika Goecke, Manfred Wilhelm, and Valerian Hirschberg*

Polymer topology highly impacts rheological melt and foaming properties. Grafting sidechains onto a linear polymer typically results in shear thinning and strain hardening in elongation flow. To study the influence of an increasing number of covalently connected polystyrene (PS) stars s with a linear PS chain ($M_{w,PS} = 90 \text{ kg mol}^{-1}$), low-disperse branched polymers with s ranging from one to four are synthesized. Each star contains approximately 12 sidechains with a length of $M_{w,a} \approx 25 \text{ kg mol}^{-1}$. Oscillatory shear measurements indicated that the zero-shear viscosity η_0 scales with $\eta_0 \approx M_{w,t}^{3.9}$ at $T_{ref} = 180 \text{ }^\circ\text{C}$. Moreover, uniaxial elongation rheology allows determining the strain hardening factor SHF , which varies between $SHF = 2\text{--}135$, with increasing s . Foaming experiments revealed that combining viscosity reduction with the improvement of stretchability promotes higher volume expansion ratios ($VER = 3.21\text{--}10.41$) and the formation of larger cells ($D = 4.8\text{--}14.8 \text{ }\mu\text{m}$).

elongational flow.^[13–15] Though, the synthesis of polymers with a defined POM-POM topology is already quite complex. Especially to investigate the influence of the molecular parameters like the molecular weight of the backbone and sidechains, or the number of sidechains, a precise and well-controlled synthesis route is essential.^[16–18] Additionally, the POM-POM topology represents the basis for the POM-POM constitutive model, developed to predict the shear, and especially the elongation behavior of commercial long-chain branched polymers in the melt state. Low-density polyethylene (LDPE) might be the most prominent example.^[14,19–24] Consequently, the rheological properties can be predicted in shear and elongational flow via molecular properties and compared to experimental data.

1. Introduction

The simplest architecture of branched polymers is a star with three to four arms. Moreover, the rheological behavior of stars is different compared to linear polymers, as the branching point changes relaxation behavior. Researchers have investigated their rheological behavior in the melt, as dilute solutions or as blends with linear polymer chains.^[1–12] In the so-called POM-POM topology, two similar stars are covalently connected with a linear polymer chain, representing the simplest topology with exactly two branching points. The POM-POM topology gained a lot of interest, as it represents the most straightforward topology, which combines shear thinning and strain hardening in

Despite the high number of publications on polymer stars and related like POM-POMs (2-stars), to the best of our knowledge, no study on multiple, chemically bonded stars, that is, barbwire type molecules, and the influence of the inherent topological parameters on the melt rheological properties and foaming behavior has been conducted.


Herein, we report a rather simple synthetic route to polymers with an increasing number of covalently connected stars s using living anionic polymerization and grafting-onto methodology and investigate the influence of s on their rheological melt properties and foaming behavior.

2. Experimental Section

2.1. Materials

Stabilized styrene (99 %, extra pure, Sigma-Aldrich) was stirred one night over calcium hydride and purified by distillation from di-*n*-butyl magnesium (0.5 M, Fisher Scientific). Stabilized isoprene (98 %, VWR) was purified by first cooling the monomer and adding *n*-butyllithium, followed by distillation into ampoules. The purified monomers were stored under an argon atmosphere at $T = -18 \text{ }^\circ\text{C}$ until needed. Cyclohexane (CH, 99%, Fisher Scientific) and toluene (> 99%, Roth) were stored over living polystyrene and distilled before use. Tetrahydrofuran (THF, 99.5%, Roth) was distilled from CaH₂, stored over sodium/benzophenone, and distilled before

M.-C. Röpert, A. Goecke, M. Wilhelm, V. Hirschberg
 Institute for Chemical Technology and Polymer Chemistry
 Karlsruhe Institute of Technology (KIT)
 Engesserstraße 18, 76131 Karlsruhe, Germany
 E-mail: valerian.hirschberg@kit.edu

 The ORCID identification number(s) for the author(s) of this article can be found under <https://doi.org/10.1002/macp.202200288>

© 2022 The Authors. Macromolecular Chemistry and Physics published by Wiley-VCH GmbH. This is an open access article under the terms of the Creative Commons Attribution License, which permits use, distribution and reproduction in any medium, provided the original work is properly cited.

DOI: 10.1002/macp.202200288

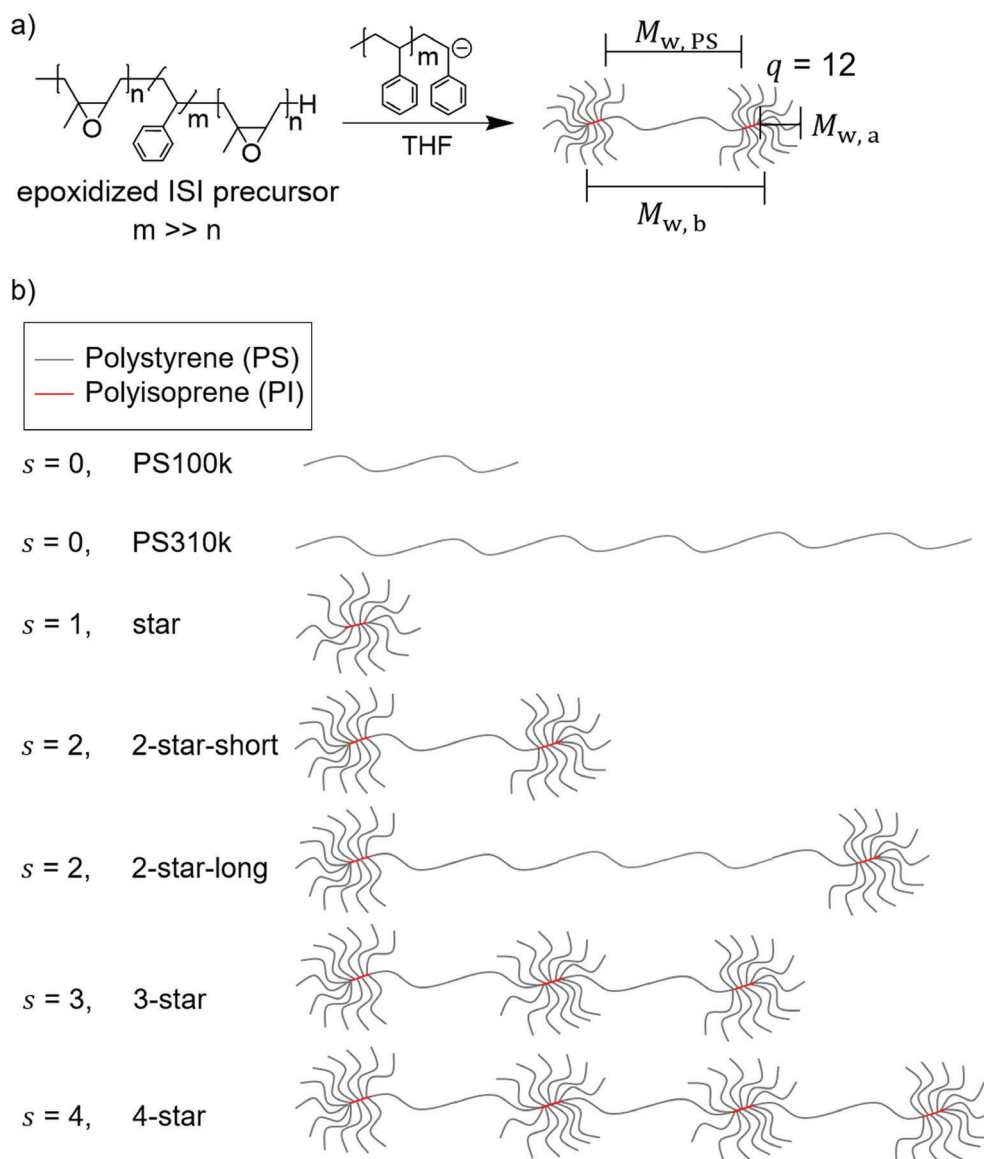


Figure 1. a) Exemplary synthesis of the POM-POM topology ($s = 2$) via a combination of living anionic polymerization and the grafting-onto methodology. b) Schematic representation of the synthesized samples: two linear PS references with molecular weights of 100 and 310 kg mol^{-1} ($s = 0$), one star ($s = 1$), two POM-POMs ($s = 2$, 2-star-short with $M_{w,b} \approx 100 \text{ kg mol}^{-1}$ and 2-star-long with $M_{w,b} \approx 280 \text{ kg mol}^{-1}$), and barbwire topologies ($s = 3, 4$) with an increasing amount of covalently connected stars s with a PS chain with $M_{w,PS} \approx 90 \text{ kg mol}^{-1}$. Grey and red lines correspond to polystyrene (PS) and polyisoprene (PI), respectively.

synthesis. 1,4-Dioxane ($\geq 99.8\%$, Fisher Scientific) was distilled to remove the stabilizer. Methanol (99%, Fisher Scientific) was degassed by three successive freezing-evacuation-thawing cycles. For SEC measurements, SEC grade THF was used (0.025% BHT, Fisher Scientific). *n*-Butyllithium (*n*-BuLi, 2.5 M in hexane, Sigma Aldrich), *s*-butyllithium (*s*-BuLi, 1.4 M in CH, Sigma-Aldrich), calcium hydride (CaH_2 , 92%, Thermo Fischer Scientific), chloroform- d_1 (CDCl_3 , 99.8%, Sigma Aldrich), formic acid ($> 98\%$, Thermo Fischer Scientific), hydrogen peroxide (H_2O_2 , 30%, Thermo Fischer Scientific), and sodium benzophenone (99%, Arcos Organics) were used as received.

2.2. Anionic Polymerization and Grafting-onto Methodology

The samples with an increasing number of covalently connected stars s were synthesized by using a combination of living anionic polymerization and grafting-onto procedure, see **Figure 1** and **Figure S1**, Supporting Information. Within the sample series, s increases systematically from one single star (star, $s = 1$) to four connected stars (4-star, $s = 4$) with a linear PS chain of $M_{w,PS} \approx 90 \text{ kg mol}^{-1}$. The backbone length $M_{w,b}$ was increased from $M_{w,b} = 7\text{--}382 \text{ kg mol}^{-1}$, depending on s . The molecular weight of the sidechains $M_{w,a}$ varies between $M_{w,a} = 22\text{--}25 \text{ kg mol}^{-1}$, and the

Table 1. Molecular characteristics of the linear PS references, the PS- and PI-based precursors, and the branched samples.

Sample	<i>s</i>	$M_{w,t}^{a)}$ [kg mol ⁻¹]	$\bar{D}t^{a)}$	<i>q</i> ^{b)}	$M_{w,a}$ [kg mol ⁻¹]	$\bar{D}a$	$Z_t^{c)}$
PS100k	–	100	1.01	–	–	–	5.95
PS310k	–	310	1.10	–	–	–	17.26
PI (precursor for <i>s</i> = 1)	–	7	1.10	–	–	–	1.56
ISI (precursor for <i>s</i> = 2)	–	100	1.05	–	–	–	7.50
ISI (precursor for <i>s</i> = 2)	–	280	1.08	–	–	–	12.30
ISISI (precursor for <i>s</i> = 3)	–	213	1.16	–	–	–	14.05
ISISI (precursor for <i>s</i> = 4)	–	382	1.35	–	–	–	20.51
Star (8k-11-27k)	1	305	1.09	11	27	1.07	19.46
2-star-short (100k-2 × 12-24k)	2	600	1.18	2 × 12	24	1.05	42.46
2-star-long (280k-2 × 13-22k)	2	852	1.17	2 × 13	22	1.08	52.94
3-star (213k-3 × 11-25k)	3	1038	1.10	3 × 11	25	1.09	65.08
4-star (382k-4 × 11-27k)	4	1570	1.14	4411	27	1.12	95.67

^{a)} Dispersities were determined from SEC-DRI signal, whereas absolute weight average molecular weights were obtained by using MALLS detection. ^{b)} Number of sidechains per star is calculated by $q = (m_s/m_t) \times (n_a/2n_b)$, with m_s as the ratio of the known mass of POM-POM, m_t as the total mass of the raw product, n_a and n_b as the ratio of the total number of added sidechains to the number of backbones.^[25] ^{c)} $M_{e,PS} = 16.8$ kg mol⁻¹, $M_{e,PI} = 4.5$ kg mol⁻¹ were used to calculate the total number of entanglement Z_t .^[26] For branched materials Z_t is calculated by the sum of the number of entanglements of the backbone and the sidechains.

number of sidechains per star was on average $q \approx 12$, as previous works of the group have revealed that this combination is suitable to study the shear and elongational rheological properties.^[25] To examine whether the impact of topology results from increasing *s* or $M_{w,b}$, the results were compared with a POM-POM with $M_{w,b} \approx 280$ kg mol⁻¹.

The star was synthesized in three steps. First, a linear PI backbone (10 mL isoprene, 99.8 mmol) was synthesized via living anionic polymerization in cyclohexane (150 mL) at room temperature with *s*-BuLi (0.97 mL, 1.36 mmol) as the initiator. Cyclohexane was used as a solvent to control the microstructure of the PI, as only 1,4-*cis* PI are epoxidizable with the conditions used.^[47] The synthesis of the PI backbone was followed by epoxidation of the double bonds with formic acid (3.75 g, 78.0 mmol) and hydrogen peroxide (8.85 g, 80.0 mmol) at 40 °C in toluene (150 mL) to functionalize the backbone for the following grafting-onto of living anionic polystyrene chains. A detailed epoxidation, grafting-onto, and synthesis procedure of the samples with *s* = 2 (2-stars, POM-POMs) could be found elsewhere.^[25,47]

The samples with *s* = 3, 4 (3-star, 4-star) were based on a penta- and hepta-block copolymer as a backbone, respectively. To synthesize the penta- and hepta-block copolymers based on PI and PS, asymmetric ISI' tri-block and ISIS' quadro-block copolymers with $I = 2 \times I'$ and $S = 2 \times S'$ in cyclohexane (200 mL) with *s*-BuLi (0.133 mL, 0.186 mmol; 0.089 mL, 0.125 mmol) as initiator at room temperature were synthesized. The length of the styrene (S) blocks corresponded to 90 kg mol⁻¹ (18.4 mL, 161 mmol), and the length of isoprene (I) blocked to 5 kg mol⁻¹ (1.34 mL, 13.38 mmol), while *S'* and *I'* were each half of S and I, respectively. After complete conversion of the ISI' and ISIS' blocks, the blocks were subsequently linked with a bifunctional linker, α, α' -dibromo-*p*-xylene (4.3 mL, 0.094 mmol; 2.9 mL, 0.063 mmol), to obtain the penta- (ISISI) and heptablock (ISISISI) copolymer, respectively. The PI parts of the backbones were functionalized by epoxidation,^[47] followed by grafting of living polystyrene sidechains onto the backbones, resulting in the 3-star and 4-star

topologies, see Figure S1, Supporting Information. The resulting polymers were purified by, on average, three fractionation steps in a mixture of THF and methanol until a purity of > 93% was reached.

The linear backbones and the branched structures were characterized by size-exclusion chromatography (SEC) and nuclear magnetic resonance (¹H-NMR) spectroscopy. The resulting molecular parameters are summarized in Table 1.

The resulting stars had an average sidechain number of $q \approx 12$, and therefore the chains could not emanate from exactly one branching point. The sidechains were statistically distributed along the PI block with $M_{w,PI} \approx 5$ kg mol⁻¹. With $q \approx 12$, the branching density averaged about one grafted sidechain every sixth isoprene unit. Hence, the stars could also be described as two connected loosely-grafted bottlebrushes.^[25]

2.3. Melt Rheological Measurements

Small-amplitude oscillatory shear (SAOS) measurements were performed from 130 to 180 °C using parallel plates with a diameter of 13 mm on an ARES-G2 rheometer (TA Instruments) under a nitrogen atmosphere to minimize polymer degradation. The master curves were obtained by using the time-temperature superposition principle and referenced to a temperature of $T_{ref} = 180$ °C.

Uniaxial elongation experiments were performed at 180 °C for strain rates in the range of $\dot{\epsilon} = 0.03$ – 10 s⁻¹ using an extensional viscosity fixture (EVF) with a maximum possible Hencky strain of $\epsilon_H = 4$.

2.4. Foaming Experiments and Characterization

Samples were foamed in a one-batch physical foaming process using supercritical carbon dioxide (scCO₂) as the foaming

agent. Samples were saturated at the foaming temperature under 500 bar for 8 h for complete saturation. Foaming temperatures varied between 100 and 150 °C, and the depressurization rate was $\approx 200 \text{ bar s}^{-1}$.

The resulting foams and their cellular structure could be described by the following parameters: foam density ρ_f , volume expansion ratio VER , average cell size D , and cell density N . The foam density was measured based on Archimedes' principle, and the VER was calculated from the ratio of the polymer density ρ_p to the foam density ρ_f . The cellular structure of the foams was analyzed via scanning electron microscopy (SEM), and the resulting images were used to calculate D and N , by using Equations (1) and (2):

$$N = (n/A)^{3/2} (VER) \quad (1)$$

$$D = 10^4 [(VER - 1) / (N\pi/6)]^{1/3} \quad (2)$$

where N is the cell density in cell cm^{-3} , n is the number of cells in an observed area A , and D is the average cell size in μm .

3. Results and Discussion

3.1. Oscillatory Shear Measurements

We performed small-amplitude oscillatory shear (SAOS) measurements at $T = 130\text{--}180 \text{ }^\circ\text{C}$ to study the influence of increasing s on the viscoelastic behavior. Figure 2a summarizes the master curves of the storage G' and loss modulus G'' as a function of the angular frequency $a_T\omega$ of some selected samples, referenced to $T_{ref} = 180 \text{ }^\circ\text{C}$. The corresponding WLF parameters and all individual master curves of the materials are available in the supporting information, see Table S1 and Figure S3, Supporting Information. At the modulus cross-over in the low-frequency regime, the whole polymer is relaxed, and consequently, the average longest relaxation time τ_l can be calculated by $\tau_l = 1/\omega$, while τ_l of the sample with $s = 1$ was determined according to literature.^[25] The resulting τ_l are depicted as a function of $M_{w,t}$ in Figure 2b. Figure 2c displays the van Gurp–Palmen plot. This way to display the viscoelastic shear response under oscillatory excitation is, at first approximation, independent of the molecular weight for a linear topology, as only the δ value of the minimum decreases with increasing molecular weight.^[27,28] Consequently, the effect of topologies is amplified, allowing us to compare the viscoelastic behavior of polymers with varying topologies like an increasing s .

The cross-over in the high-frequency area ($\omega = 10^4\text{--}10^5 \text{ rad s}^{-1}$, for $T_{ref} = 180 \text{ }^\circ\text{C}$) of the master curves in Figure 2a can be attributed to the local segmental relaxation of the styrene units.^[19] The relaxation process of branched structures follows a hierarchical order.^[21,22] Hence, the sidechains relax first at lower temperatures, that is, higher frequencies. Therefore, the adjacent rubber plateau ($\omega \approx 10^2\text{--}10^3 \text{ rad s}^{-1}$) is caused by entangled sidechains, while the cross-over at around $\omega \approx 210 \text{ rad s}^{-1}$ can be attributed to the sidechain relaxation time τ_a . As all branched materials have similar $M_{w,a}$, τ_a for all branched samples is around $\tau_a \approx 0.03 \text{ s}$; except for the single star, where $\tau_a \approx 0.004 \text{ s}$.

The 2-star-short shows one rubber plateau caused by the sidechains and a regime, where G' and G'' are parallel with a

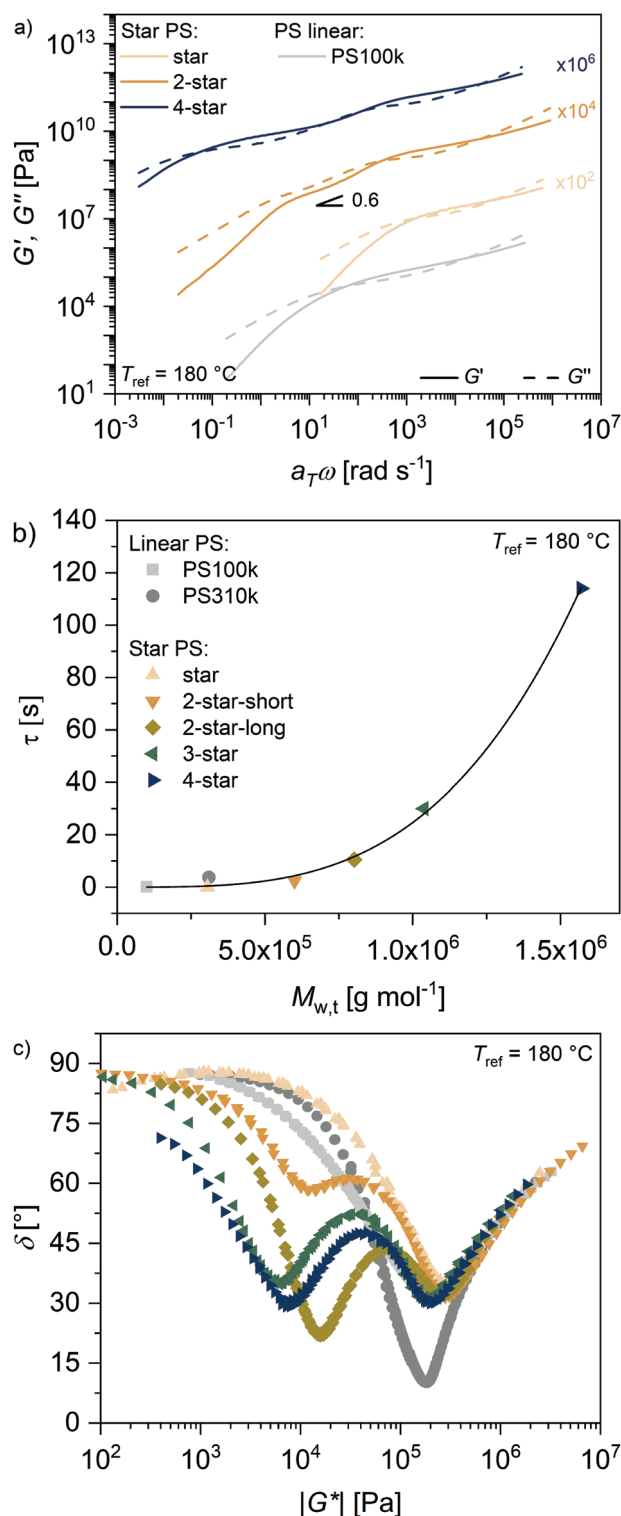


Figure 2. In (a) the master curves of the samples with an increasing number of covalently connected stars s from one to four are shown at a reference temperature of $T_{ref} = 180 \text{ }^\circ\text{C}$, indicating an asymptotic behavior in the flow region according to the Maxwell model. The master curves are vertically shifted by a factor of 10^2 , 10^6 , 10^8 , 10^{10} , 10^{12} , and 10^{14} . In (b) is the average longest relaxation time τ_l plotted against the total weight average molecular weight $M_{w,t}$ at $T_{ref} = 180 \text{ }^\circ\text{C}$. The black solid line represents a non-linear least-square fit according to a simple power law, where $M_{w,t}$

scaling exponent of 0.6 in a double-logarithmic plot. A slope of 0.6 indicates, that the backbone exhibits constraint release Rouse-like behavior instead of reptational mechanism.^[18,29–32] We attribute this phenomenon to the entangled sidechains, which entangle with the backbone and prevent the backbone from becoming entangled with itself, resulting in the absence of the backbone's rubber plateau.^[25] By lengthening the backbone to $M_{w,b} \approx 280 \text{ kg mol}^{-1}$, the backbone entangles with each other. For the samples with $s = 3, 4$, two rubber plateaus occur, indicating that sidechains and backbones are entangled. Moreover, the cross-over in the low-frequency regime can be attributed to τ_l , which increases exponentially from $4 \times 10^{-3} \text{ s}$ to 114 s ($T_{ref} = 180 \text{ }^\circ\text{C}$) with increasing $M_{w,t}$, as shown in Figure 2b. The scaling of τ_l with $\tau_l \approx M_{w,t}^{3.4}$ is regardless of whether the increased $M_{w,t}$ is due to the backbone's extension or to an additional linked star.

In Figure 2c, the observed local minima at $|G^*| = 6000\text{--}15\,000 \text{ Pa}$ for the branched topologies are related to the backbone as it is diluted by the sidechains. The second minimum in d at $|G^*| \approx 200\,000 \text{ Pa}$, a typical value for PS, is related to the entangled sidechains, corresponding to the rubber plateau.^[27,28] The phase angle at the local minimum caused by the backbone decreases continuously with increasing s from $\delta = 58^\circ$ (2-star-short) to $\delta = 29^\circ$ (4-star) if the distance between the two covalently connected stars remains the same. By extending the distance, the minimum of δ occurs at lower values with $\delta = 22^\circ$ (2-star-long). The phase angle of the sidechains' minimum is about $\delta \approx 32^\circ$, confirming similar $M_{w,a}$ for the branched structures investigated. Additionally, δ of the linear topology decreases from $\delta = 32^\circ$ to 10° with increasing $M_{w,t}$, as expected.^[27,28]

It is well-known, that branching highly impacts the viscosity of polymers, as short sidechains act as a plasticizer, reducing η_0 of the polymer melt.^[21,22] We determined η_0 and applied the multi-mode Maxwell model to G' and G'' , considering the relaxation process of both the sidechains and the backbone to determine the LVE regime. Figure 3 illustrates η_0 as a function of $M_{w,t}$; $|\eta_{(\omega)}^*|$ as a function of $a_T\omega$ and the Maxwell-modes are included in the SI, see Figure S4 and Table S2, Supporting Information, respectively.

The sidechains dramatically reduce η_0 compared to linear PS with the same $M_{w,t}$. For instance, the star has 500 times lower η_0 compared to linear PS310k. Moreover, 2-star-short has a similar η_0 as the linear PS100k, which corresponds to the M_w of the backbone, although $M_{w,t}$ is six times higher.

The zero-shear viscosity of linear homopolymer melts follows a power-law dependency with increasing molecular weight with $\eta_0 \approx M_w^{3.4}$, as known from reptation theory for $M_w > M_c$.^[35] The sample series with increasing s show a scaling behavior of $\eta_0 \approx M_w^{3.9}$, which is nearly the same as for linear polymers with increasing molecular weights, but with an overall viscosity reduction by a factor of 500. Moreover, the η_0 of the 2-star-long does not follow the trend compared to the other branched materials with a shorter backbone.

is given in g mol^{-1} (scaling exponent = 3.4, prefactor = 1×10^{-20}). In (c) is the van Gurp–Palmen plot presented. Two linear PS with molecular weights of 100 kg mol^{-1} (light grey) and 310 kg mol^{-1} (dark grey) were used as a comparison originating from a linear topology.

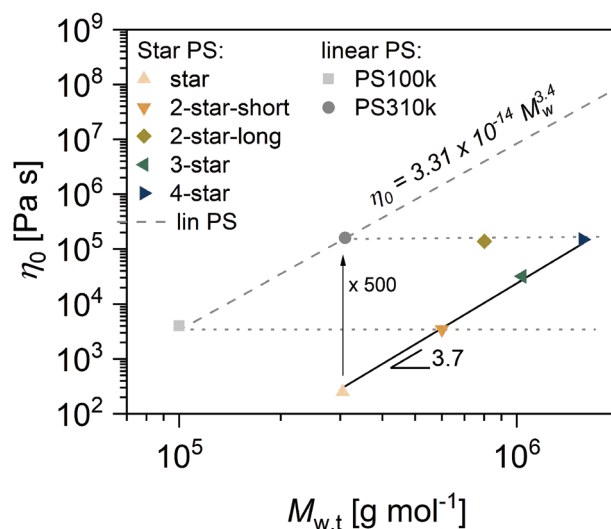


Figure 3. The zero-shear viscosity η_0 as a function of the total weight average molecular weight of the multi-stars $M_{w,t}$. The dark grey dashed line represents the prediction for linear PS from literature and scales with $\eta_0 \approx M_w^{3.4}$ (prefactor = 3.31×10^{-14}).^[34] The solid black line represents a non-linear least-square fit according to a simple power law, where $M_{w,t}$ is given in g mol^{-1} (scaling exponent = 3.9, prefactor = 1×10^{-19}). Light grey dotted horizontal lines are to guide the eye.

3.2. Uniaxial Elongation Measurements

Elongation measurements were performed to investigate the melt properties under uniaxial stretching. The experiments were conducted at $180 \text{ }^\circ\text{C}$ between strain rates of $\dot{\epsilon} = 10\text{--}0.003 \text{ s}^{-1}$. A parameter to evaluate the elongation capability is the strain hardening factor SHF , which is described by the ratio of the maximum measured tensile stress growth coefficient $\eta_{E,max}^+(t, \dot{\epsilon}_H)$ to the theoretical viscoelastic linear response predicted using the Doi–Edwards model (DE) $\eta_{E,DE}^+(\dot{\epsilon}_H)$.^[36] The software IRIS Rheo-Hub of Mours and Winter,^[37,38] enabling to extend linear and non-linear rheological measurements by predicting theories, was used to calculate the Doi–Edwards model. Figure 4a shows the viscosity growth curves of the 4-star at $T = 180 \text{ }^\circ\text{C}$; curves of all samples are represented in Figure S5, Supporting Information. Figure 4b provides the resulting SHF as function of $\dot{\epsilon}$ and the reached values are summarized in Table S3, Supporting Information.

No elongation measurement could be performed with PS100k and the single star as the viscosities were too low at $T = 180 \text{ }^\circ\text{C}$. However, no strain hardening is expected for a star-like topology, as it has only one branching point. At least two spatially separated branching points are required to generate strain hardening in elongational flow, for example, in H-shaped or POM-POM topology.^[14,20] The linear PS310k shows a minor SHF of $SHF = 2$ at $\dot{\epsilon} = 10$.

By increasing $M_{w,b}$ from $M_{w,b} \approx 100\text{--}280 \text{ kg mol}^{-1}$, but keeping $s = 2$, the maximum SHF massively increases from $SHF = 7$ to ≈ 100 , respectively. The distinct difference between these two samples is justified in the backbones' entanglement number. For $s = 2$, only the backbone of the sample with $M_{w,b} \approx 280 \text{ kg mol}^{-1}$ is entangled with other backbones, confirmed by

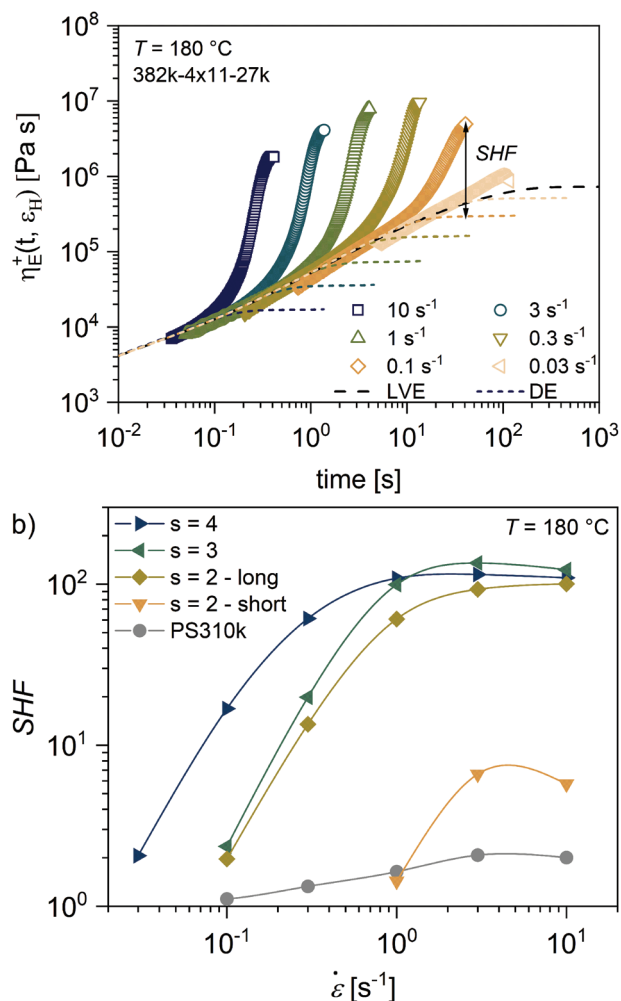


Figure 4. a) Viscosity growth curves of the 4-star measured at elongation strain rates $\dot{\epsilon}$ ranging from 0.03 to 10 s⁻¹ at $T = 180$ °C. Dashed and dotted lines represent the linear viscoelastic (LVE) regime and the Doi–Edwards (DE) model, respectively.^[36,39,40] b) Strain hardening factors SHF of all samples as a function of the elongational strain rate $\dot{\epsilon}$. As the elongational viscosity of both, the star ($s = 1$) and the short linear PS100k reference, was too low, and therefore, the elongation viscosity could not be measured; no data are included in the graph. The lines are guides to the eyes.

the rubber plateau in the low-frequency regime, see Figure 2a. Thus, the entanglement of both the backbone and the sidechains contributes to the SHF , resulting in a significant increase, while for the sample with $M_{w,b} \approx 100$ kg mol⁻¹ and $s = 2$ only the entanglement with the sidechains contributes to the SHF . The addition of even more stars along the backbone has a minor influence, as $SHF = 135$ and 114 for $s = 3$ and 4, respectively. Therefore, a minimum of a single backbone with several entanglements between two branching points seems to be the critical parameter for extreme strain hardening in branched topologies. Furthermore, the SHF decreases with decreasing $\dot{\epsilon}$ for all materials, and the minimum $\dot{\epsilon}$, where strain hardening still occurs decreases with increasing s .

3.3. Physical Batch Foaming

Materials combining strain hardening in elongational flow at $\dot{\epsilon} = 10$ – 1 s⁻¹ with a low η_0 in shear are highly suitable for foaming polymers, as they support foamability by reducing cell coalescence and rupture.^[41–45] The presented series meets both criteria, hence, we tested the samples regarding their foaming behavior.

The samples were foamed at temperatures between 100–150 °C with supercritical carbon dioxide (scCO₂) as a foaming agent under a pressure of 500 bar. The SEM images of the foams at $T = 140$ °C (a) and a selective part of the complete data are depicted in Figure 5, displaying the b) VER and the c) D as a function of s , foamed at $T = 100$ – 140 °C. At higher temperatures, the foams collapsed. The complete statistical results of the foam density ρ_f , volume expansion ratio VER , average cell size D , and nucleation density N are summarized in the supporting information, see Table S4, Supporting Information.

The VER and D increase with increasing foaming temperature until the foams collapse. The foams based on the linear PS310k and single star collapsed at $T = 130$ °C. In contrast, the multi-stars were foamable up to $T = 150$ °C, underlining the importance of topology and the requirement of at least two branching points, resulting in high melt strength, that is, strain hardening. The single star ($s = 1$) exhibits VER of $VER = 2.63$ – 5.35 within $T = 100$ – 130 °C. In combination with the formation of relatively large cells with $D = 6.8$ – 11.2 μm , compared to the other branched samples, the experiments revealed that the significantly lower η_0 and the low melt strength of the star lead to an increased tendency for cell coalescence.

At lower temperatures, no significant difference of VER occurs over the entire samples. As soon as the foaming temperature rises, the foams based on the multi-stars ($s = 2$ – 4) expand significantly more than the linear PS and the star. The maximum reached VER of the linear PS and the star are $VER = 5.45$ and 5.35 at $T = 130$ °C, respectively, while the multi-stars reached $VER = 8.85$ – 10.41 at $T = 140$ °C.

However, an increasing s has a tremendous impact on D , which is also more pronounced at higher temperatures. At lower foaming temperatures, the resulting D of the 4-star is smaller than D of 3-star, as it combines the highest η_0 of $\eta_0 \approx 148$ 000 Pa s ($s = 4$) compared to $\eta_0 \approx 31$ 000 Pa s ($s = 3$) and the highest overall amount of entanglements of $Z_e \approx 95$, suppressing the cell growth rate and resulting in smaller cell sizes.^[41,46] Nevertheless, the effect is minimized at $T = 140$ °C, and thus, D increases significantly with increasing s from 6.3 μm ($s = 2$, short) to 14.8 μm ($s = 4$), revealing that lower viscosities promote higher VER and the formation of larger cells, due to the reduced viscosity-driven resistance to cell growth. These findings are in agreement with the literature, for instance, it was shown by numerical analysis, that the cell growth rate is strongly affected by the viscosity variation during the initial step of cell growth.^[46]

4. Conclusion

In summary, we have synthesized rather simple, well-defined branched polystyrenes (PS) with increasing s (each 12 arms, $M_{w,a} \approx 25$ kg mol⁻¹) ranging from one to four with a fixed molecular weight between the stars of $M_{w,PS} \approx 90$ kg mol⁻¹ via combining living anionic polymerization with grafting-onto method-

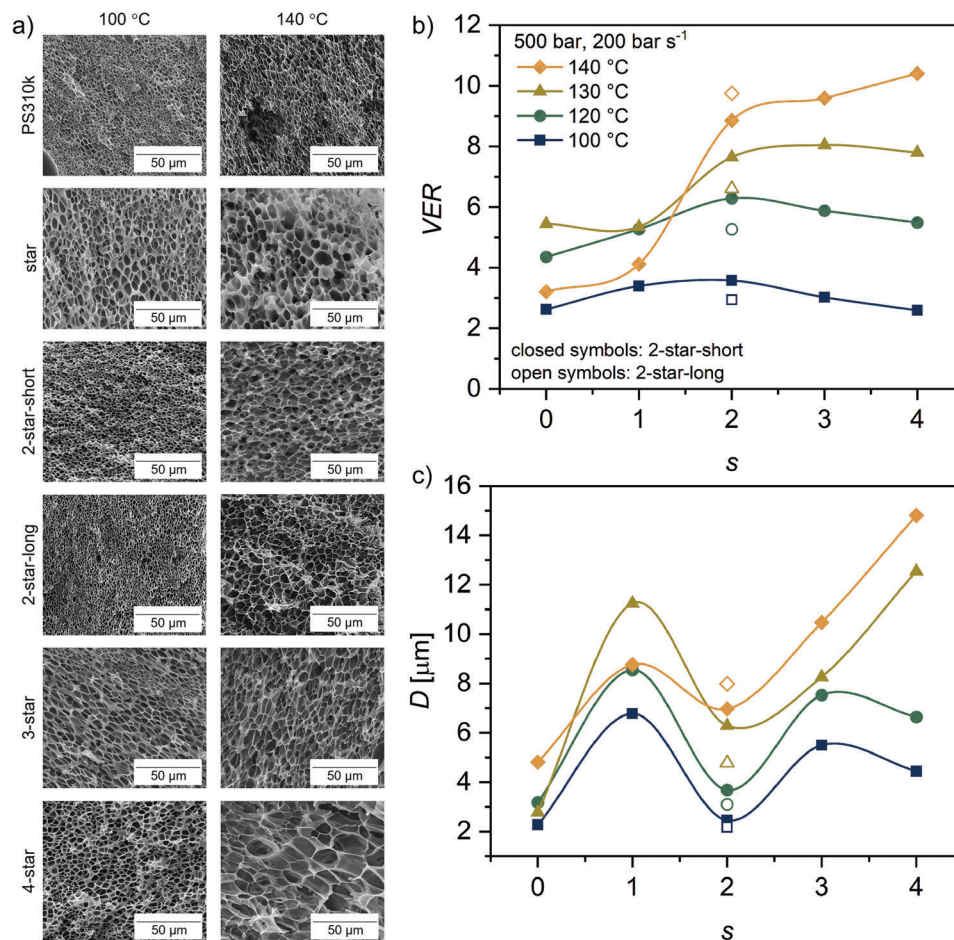


Figure 5. a) SEM images of the linear PS310k and the branched samples foamed at $T = 140$ °C. b) Volume expansion ratio VER and c) average cell diameter D as a function of the number of connected stars s foamed at 500 bar with a depressurization rate of about 200 bar s^{-1} in a temperature range of $T = 100$ – 140 °C.

ology. Oscillatory-shear measurements indicate, that the average longest relaxation time of the materials increases exponentially from $\tau_1 = 4 \times 10^{-3}$ s to 114 s with increasing $M_{w,t}$ at $T_{ref} = 180$ °C. Moreover, η_0 of the branched samples scales with $\eta_0 \approx M_{w,t}^{3.9}$, which is similar to the expected slope of 3.4,^[35] but reduced by a factor of 500 compared to linear PS with the same $M_{w,t}$. The SHF , measured by uniaxial elongation measurements, increases drastically from $SHF = 7$ – 114 , as a function of s at $T = 180$ °C. Moreover, the samples were physically foamed with scCO_2 at 500 bar and temperatures between 100 and 150 °C to study their foaming potential. The experiments demonstrate that the introduction of sidechains increased melt strength and thus improved VER and cell stabilization. For instance, while VER increases with increasing s from $VER = 5.45$ to 10.41, D shows a local minimum for both samples with $s = 2$ at each investigated temperature. Moreover, at $T = 140$ °C, D increases with from $D = 6.9 \mu\text{m}$ ($s = 2$, short) to $D = 14.8 \mu\text{m}$ ($s = 4$). At lower foaming temperatures, the high number of entanglements and the resulting increased η_0 of $s = 4$ slowed down the cell growth rate, resulting in smaller cells than the samples with fewer s .

These findings highlight the importance of controlling the polymers' topology and the associated rheological melt proper-

ties in shear and elongational flow to achieve the desired cellular structure of the resulting polymer foams.

Supporting Information

Supporting Information is available from the Wiley Online Library or from the author.

Acknowledgements

The authors gratefully acknowledge the DECHEMA's Max Buchner Research Foundation for the research grant. The authors thank Ingrid Zeller for helping with SEM measurements. Furthermore, the authors thank Prof. H. Henning Winter for access to IRIS Rheo-Hub software.

Open Access funding enabled and organized by Projekt DEAL.

Conflict of Interest

The authors declare no conflict of interest.

Data Availability Statement

The data that support the findings of this study are available in the supplementary material of this article.

Keywords

melt rheology, physical foaming, polymer topology, strain hardening factor, structure-property relationship

Received: August 10, 2022

Revised: September 10, 2022

Published online:

- [1] L. J. Fetters, A. D. Kiss, D. S. Pearson, G. F. Quack, F. J. Vitus, *Macromolecules* **1993**, *26*, 647.
- [2] C. H. Adams, L. R. Hutchings, P. G. Klein, T. C. B. Mcleish, R. W. Richards, *Macromolecules* **1996**, *29*, 5717.
- [3] N. Hadjichristidis, *J. Polym. Sci., Part A: Polym. Chem.* **1999**, *37*, 857.
- [4] T. Higashihara, R. Faust, K. Inoue, A. Hirao, *Macromolecules* **2008**, *41*, 5616.
- [5] J. H. Lee, K. Orfanou, P. Driva, H. Iatrou, N. Hadjichristidis, D. J. Lohse, *Macromolecules* **2008**, *41*, 9165.
- [6] A. Miros, D. Vlassopoulos, A. E. Likhtman, J. Roovers, *J. Rheol.* **2003**, *47*, 163.
- [7] S. Hietala, P. Mononen, S. Strandman, P. Järvi, M. Torkkeli, K. Jankova, S. Hvilsted, H. Tenhu, *Polymer* **2007**, *48*, 4087.
- [8] S. Hietala, S. Strandman, P. Järvi, M. Torkkeli, K. Jankova, S. Hvilsted, H. Tenhu, *Macromolecules* **2009**, *42*, 1726.
- [9] V. Metri, A. Louhichi, J. Yan, G. P. Baeza, K. Matyjaszewski, D. Vlassopoulos, W. J. Briels, *Macromolecules* **2018**, *51*, 2872.
- [10] E. V. Ruymbeke, E. B. Muliawan, D. Vlassopoulos, H. Gao, K. Matyjaszewski, *Eur. Polym. J.* **2011**, *47*, 746.
- [11] Q. Huang, S. Agostini, L. Hengeller, M. Shivokhin, N. J. Alvarez, L. R. Hutchings, O. Hassager, *Macromolecules* **2016**, *49*, 6694.
- [12] M. H. Wagner, E. Narimissa, Q. Huang, *Rheol. Acta* **2022**, *61*, 415.
- [13] H. Lentzakis, D. Vlassopoulos, D. J. Read, H. Lee, T. Chang, P. Driva, N. Hadjichristidis, *J. Rheol.* **2013**, *57*, 605.
- [14] T. C. B. Mcleish, R. G. Larson, *J. Rheol.* **1998**, *42*, 81.
- [15] N. J. Inkson, T. C. B. Mcleish, O. G. Harlen, D. J. Groves, *J. Rheol.* **1999**, *43*, 873.
- [16] M. Kempf, V. C. Barroso, M. Wilhelm, *Macromol. Rapid Commun.* **2010**, *31*, 2140.
- [17] M. Kempf, D. Ahirwal, M. Cziep, M. Wilhelm, *Macromolecules* **2013**, *46*, 4978.
- [18] M. Abbasi, L. Faust, K. Riazi, M. Wilhelm, *Macromolecules* **2017**, *50*, 5964.
- [19] J. M. Dealy, D. J. Read, R. G. Larson, *Structure and Rheology of Molten Polymers: From Structure to Flow Behavior and Back Again*, 2nd ed., Hanser Publications, Cincinnati, OH **2018**.
- [20] T. C. B. Mcleish, J. Allgaier, D. K. Bick, G. Bishko, P. Biswas, R. Blackwell, B. Blottière, N. Clarke, B. Gibbs, D. J. Groves, A. Hakiki, R. K. Heenan, J. M. Johnson, R. Kant, D. J. Read, R. N. Young, *Macromolecules* **1999**, *32*, 6734.
- [21] T. C. B. Mcleish, *EPL* **1988**, *6*, 511.
- [22] T. C. B. Mcleish, *Adv. Phys.* **2002**, *51*, 1379.
- [23] I. Vittorias, M. Parkinson, K. Klimke, B. Debbaut, M. Wilhelm, *Rheol. Acta* **2006**, *46*, 321.
- [24] P. Rubio, M. Wagner, *J. Non-Newtonian Fluid Mech.* **2000**, *92*, 245.
- [25] M.-C. Röpert, M. G. Schußmann, M. K. Esfahani, M. Wilhelm, V. Hirschberg, *Macromolecules* **2022**, *55*, 5485.
- [26] M. A. Cziep, M. Abbasi, M. Heck, L. Arens, M. Wilhelm, *Macromolecules* **2016**, *49*, 3566.
- [27] S. Trinkle, C. Friedrich, *Rheol. Acta* **2001**, *40*, 322.
- [28] S. Trinkle, P. Walter, C. Friedrich, *Rheol. Acta* **2002**, *41*, 103.
- [29] J. D. Ferry, *Viscoelastic Properties of Polymers*, 3rd ed., Wiley, New York **1980**.
- [30] C. M. Roland, L. A. Archer, P. H. Mott, J. Sanchez-Reyes, *J. Rheol.* **2004**, *48*, 395.
- [31] W. F. M. Daniel, J. Burdyńska, M. Vatankhah-Varnoosfaderani, K. Matyjaszewski, J. Paturej, M. Rubinstein, A. V. Dobrynin, S. S. Sheiko, *Nat. Mater.* **2016**, *15*, 183.
- [32] C. Bailly, V. Stephenne, Z. Muchtar, M. Schappacher, A. Deffieux, *J. Rheol.* **2003**, *47*, 821.
- [33] F. A. Morrison, *Understanding Rheology: Topics in Chemical Engineering*, Oxford University Press, New York **2001**.
- [34] J. Hepperle, H. Münstedt, P. K. Haug, C. D. Eisenbach, *Rheol. Acta* **2005**, *45*, 151.
- [35] G. C. Berry, T. Fox, *Adv. Polym. Sci.* **1968**, *5*, 261.
- [36] M. Rubinstein, R. H. Colby, *Polymer Physics*, Oxford University Press, New York **2003**.
- [37] H. H. Winter, M. Mours, *Rheol. Acta* **2006**, *45*, 331.
- [38] L. Poh, E. Narimissa, M. H. Wagner, H. H. Winter, *Rheol. Acta* **2022**, *61*, 259.
- [39] V. H. Rolón-Garrido, *Rheol. Acta* **2014**, *53*, 663.
- [40] F. H. Wagner, M. Yamaguchi, M. Takahashi, *J. Rheol.* **2003**, *47*, 779.
- [41] R. Liao, W. Yu, C. Zhou, *Polymer* **2010**, *51*, 568.
- [42] M. Abbasi, L. Faust, M. Wilhelm, *Polymer* **2020**, *193*, 122354.
- [43] E. Bahreini, S. F. Aghamiri, M. Wilhelm, M. Abbasi, *J. Cell. Plast.* **2018**, *54*, 515.
- [44] J. Stange, H. Münstedt, *J. Cell. Plast.* **2006**, *42*, 445.
- [45] J. Stange, H. Münstedt, *J. Rheol.* **2006**, *50*, 907.
- [46] M. Ataei, V. Shaayegan, C. Wang, F. Costa, S. Han, C. B. Park, M. Bussmann, *J. Rheol.* **2019**, *63*, 895.
- [47] Z. Yuan, M. Gauthier, *Macromolecules* **2005**, *38*, 4124.